AIAA JOURNAL
Vol. 43, No. 12, December 2005

Experimental Study on Aerodynamic Characteristics of Unsteady Wings at Low Reynolds Number

M. Okamoto*
Wakayama Technical High School, Wakayama 641-0036, Japan
and
A. Azuma†
University of Tokyo, Kawasaki 212-0021, Japan

Aerodynamic forces and moment acting on wings of AR = 6 with heaving and feathering oscillations in a wind tunnel were measured at a low Reynolds number less than 10^4. Airfoils of the wings examined are not streamlined, but they are in various profiles such as a flat plate with and without sharp leading edge, circular arc, and corrugated airfoils. By analyzing the sinusoidal aerodynamic forces and moment, it was found that some differences among airfoils were remarkable in both the mean values and the first harmonic amplitude of aerodynamic coefficients. A large perpendicular force is obtained in some airfoils, but the thrust was almost canceled by the drag in this low-Reynolds-number range during heaving motion alone. To get the maximum thrust, the optimal phase shift of combined heaving and feathering motion was required.

Nomenclature

AR	=	aspect ratio, b^2/S
a_0	=	lift slope of two-dimensional wing
b	=	span length
$C_{()}$	=	coefficients of force and moment related to ( )
c	=	chord length
D	=	drag of three-dimensional wing
f	=	frequency, Hz
h	=	heaving displacement (positive downward)
k	=	reduced frequency, $\omega c/2U$
L	=	lift of three-dimensional wing
M	=	pitching or feathering moment of three-dimensional wing
m	=	mass of wing
P	=	perpendicular force of three-dimensional wing
R	=	resultant aerodynamic force of three-dimensional wing
r	=	distance between feathering axis and center of gravity
S	=	wing area
T	=	thrust of three-dimensional wing
t	=	thickness; time
U	=	horizontal velocity
V	=	inflow velocity
(x, z)	=	two-dimensional inertial coordinate frame
α	=	angle of attack
Δx	=	distance between aerodynamic center and chordwise position about which the moment is measured
θ	=	pitch or feathering angle
ρ	=	air density
φ	=	inflow angle, $\tan^{-1}(\dot{h}/U)$
ψ_P, ψ_T, ψ_M, ψ_L	=	phase shifts of C_P, C_T, C_M, C_L, respectively, with respect to the heaving
ψ_θ, ψ_α	=	phase difference of feathering with respect to the heaving height h
ω	=	angular velocity

Subscripts

I	=	inertial component
M	=	measured value
max	=	maximum value
min	=	minimum value
( )	=	representation of D, L, M, P, T

Introduction

MANY theoretical studies on two-dimensional aerodynamic characteristics of unsteady wings in high-Reynolds-number flow have been conducted during the studies of airplane wing fllutter. However, in low-Reynolds-number flow ($Re < 10^4$), such as the flight of insects, the experimental study as well as the theoretical study on aerodynamics of steady and unsteady wings are limited to some special cases.

Okamoto et al.[1] and Azuma et al.[2] conducted wind-tunnel tests of wings with various airfoils in steady motion at $Re \leq 10^4$. These results show that the aerodynamic characteristics of two-dimensional wings in low-Reynolds-number flow are different from those obtained in high-Reynolds-number flow. Sunada et al.[3] performed the towing test in water basin and attained the similar results.

In the experimental study of a two-dimensional unsteady wing, Dickinson and Götz[4] and Dickinson[5] conducted tests for step responses of the fluid dynamic forces of some airfoils in translational and rotational motions. Sunada et al.[6] performed tests using a flat rectangular plate in sinusoidal motion with the combination of plunging and pitching oscillation to simulate the beating wing of hovering insect and obtained sinusoidal response of fluid dynamic forces and moment.

These previous studies revealed that the unsteady forces were larger than those estimated by quasi-steady analysis, and the cause of the high lift was the result of the separated vortex reattaching to the wing during its rotation from the end to the start of a stroke. Dickinson and Götz[4] also found that the presence of camber and increased surface roughness did not increase the performance of a thin and smooth flat plate.

Many experimental tests of three-dimensional wings in unsteady motion were conducted by Zanker and Götz,[7] Ellington et al.,[8] Lehmann and Dickinson,[9] Dickinson et al.,[10] Sane and Dickinson,[11] Usherwood and Ellington,[12,13] and Srygley and Thomas.[14] Almost all wings used in the preceding experimental tests were limited to a specified wing, such as drosophila or hawkmoth, in hovering flight.

Received 22 December 2004; revision received 26 May 2005; accepted for publication 27 May 2005.

*Instructor, Department of Mechanical Engineering, 3-6-1 Nishihama.
†Professor Emeritus, Department of Engineering, 37-3 Miyako-cho, Saiwai-ku. Senior Member AIAA.

Here, again, every result confirmed that the unsteady lift generation is strongly related to the vortex bubble caused by the separated flow at the leading edge, the rotational motion at the opposite ends of both down- and upstrokes, and the vortex behavior in the wake.

The aerodynamic characteristics of a less flexible wing in steady motion are affected by three-dimensional wing configuration, spanwise distribution of two-dimensional wing section, or profile, and planform of the wing. The aerodynamic forces and moment acting on a large-aspect-ratio wing are determined mainly by the airfoil used for the wing, whereas those of a low-aspect-ratio wing are not only governed by the profile but also by the planform of the wing. As the aspect ratio decreases, the effect of planform begins to play major role on the aerodynamic characteristics. Specifically, for wings with aspect ratio less than two, the effects of planform are more significant than the effects of profile. Although the effects of the profile and planform cannot be clearly distinguished because of the nonlinear characteristics of flow expressed by the Navier–Stokes equation, the profile effects of large-aspect-ratio wing are recognized physically. These facts are known widely for fixed wing in steady motion and must be also true for the wing in unsteady motion.

In the beating motion of the wings of birds, insects, and other animals, the motion is considered to consist of flapping motion (nearly normal to the wing chord), lead-lag motion (nearly parallel to the wing chord), and the feathering motion about a spanwise axis, which does not always coincide with the axis of aerodynamic center (ac). In very strict aerodynamic sense, these motions cannot be treated separately, but they can be handled approximately to consist of heaving or plunging motion (nearly normal to the wing chord), swaying motion (nearly parallel to the wing chord), and the feathering or pitching motion about the ac at an arbitrary spanwise station.

The present study on unsteady wing is to investigate the aerodynamic characteristics of two-dimensional wings quantitatively rather than qualitatively, first in heaving and feathering motions, then to extend it to three-dimensional wings in fanning motion consisting of heaving and feathering motions, and lastly in beating motion in near future. In this paper, the aerodynamic data for thin rectangular plates, cambered plates, and corrugated plates in sinusoidal motion in uniform flow are systematically obtained. The results presented here are believed to be useful to obtain the aerodynamic forces and moment of actual three-dimensional wings based on the blade element theory.

Experimental Materials and Methods

Shown in Figs. 1 and 2 are respectively the load measuring device and driving mechanism to generate sinusoidal heaving and feathering oscillations to a model in a wind tunnel (see the detail in Ref. 1). The wind-tunnel test section is 360×360 mm square, and the airspeed was 3.7 m/s during the tests.

Shown in Figs. 3a and 3b are the combined arrangement for these oscillations shown in Figs. 1 and 2. The feathering oscillation is induced elastically through the heaving oscillation by shifting the center of gravity of the model.

Wings with eight profiles shown in Fig. 4 are all rectangular in planform with the wing chord of $c = 30$ mm, the aspect ratio of $AR = 6$, and the thickness ratio of $t/c = 5\%$. They are made of balsa, and they were used to get the aerodynamic characteristics of steady and unsteady wings at the Reynolds number of $Re = 8 \times 10^3$.

The heaving oscillation was performed by giving a vertical sinusoidal motion to the measuring device on which the model was mounted (Fig. 1b). The motion was produced by a resonant oscillation tuned with the natural frequency of the driving mechanism, which consists of a link mechanism including an eccentric mass, a coil spring, and a driving motor. A laser Doppler velocimeter was utilized to keep the amplitude of oscillation at a specified value.

The measuring device is a set of load cells (Fig. 1c). The load cells A and B consist of two aluminum blocks on which four strain gauges are attached to measure the horizontal and vertical forces, and the load cell C is made of a thin aluminum plate on which two strain gauges are attached to measure the feathering moment. However, any moving part riding on the measuring device generates inertial force and moment, which are caused by the sinusoidal heaving and feathering oscillation of the wing. To get the aerodynamic forces and moment acting on the model, the inertial force (subscript I) must be subtracted from the measured data (subscript M). That is, perpendicular and thrust components P and T of the resultant aerodynamic force R with respect to the inflow velocity and feathering moment M about the measured position are, then, given by

$$P = P_M - P_I, \qquad T = T_M - T_I$$

$$M = M_M - M_I, \qquad R = \sqrt{P^2 + T^2} \tag{1}$$

To avoid the inertial effect of the wing, the dummy cells A′, B′, C′, which are made of the same material and in the same form as the load cells A, B, C, are arranged in parallel to A, B, C. A dummy that simulates the mass of the model is utilized to cancel the inertial load acting on the wing and the other related parts. Further, the additional second harmonics of tangential force is also canceled by the preceding method. This tangential force was the centrifugal force generated by a gentle circular-arc motion of the model, which was caused by the link mechanism of the driving system for heaving motion.

The load cell output signals were analyzed by a bridge circuit, a dynamic strain analyzer (6M92, NEC) and 16-bit AD converter (AMD-5698BPC, MICRO SCIENCE), and recorded by a personal computer (PC9821, NEC). The minimum readable values were 3×10^{-4} N and 3×10^{-6} N·m, and the maximum bias error of the output signal was less than 0.05% for forces and 0.5% for moment in the full scale of the load. The interference between sensors was confirmed to be small. The natural frequency of the measuring system was more than 200 Hz.

The feathering motion can be introduced either by driving a pitching motion actively (Fig. 2) or by introducing a free pitching motion passively through the forced heaving motion (Figs. 3a and 3b).

To minimize the interference between the inertial force caused by the feathering motion and the perpendicular component of aerodynamic force, a dummy mass was installed on the wing to fix the center of gravity of the model at the feathering axis of the driving mechanism. In the combined driving system of heaving and feathering oscillations, the feathering oscillation was induced passively through the forced heaving oscillation. Thus, in the combined motion the feathering amplitude θ_1 and the phase difference between the heaving and the feathering motions ψ_θ are not arbitrary but severely restricted. Further, because of the shift of the center of gravity as shown in Fig. 3b, the induced feathering oscillation is introduced. And the following inertial forces are generated:

$$\Delta P_I = -mr\frac{\mathrm{d}^2}{\mathrm{d}t^2}\sin\theta, \qquad \Delta T_I = -mr\frac{\mathrm{d}^2}{\mathrm{d}t^2}(1-\cos\theta) \tag{2}$$

The preceding inertial forces must be subtracted from the measured values.

If a wing in a horizontal velocity U is subjected to unsteady motions such as heaving oscillation h and feathering oscillation θ with an angular velocity ω as shown in Fig. 5, then lift L, drag D, and moment M_{ac} about the aerodynamic center can be given, respectively, by

$$L = P\cos\varphi + T\sin\varphi, \qquad D = P\sin\varphi - T\cos\varphi$$

$$M_{\mathrm{ac}} \cong M - (P\cos\theta - T\sin\theta)\Delta x \tag{3}$$

where φ is the inflow angle defined later by Eq. (4) and Δx is the chordwise distance between the ac and the chordwise position where the moment is measured.

Every aerodynamic quantity is considered to be a function of the angle of attack α:

$$\alpha = \theta + \varphi, \qquad \varphi = \tan^{-1}(\dot{h}/U) \tag{4}$$

where the heaving and feathering oscillations are expressed in the following Fourier expansion series:

$$h = h_1\cos(\omega t)$$

$$\theta = \theta_0 + \theta_1\cos(\omega t + \psi_{\theta,1}) + \theta_2\cos(2\omega t + \psi_{\theta,2}) \tag{5}$$

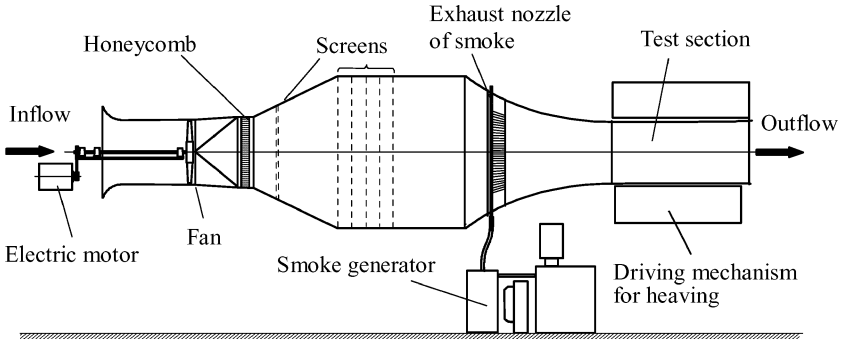

a) Wind tunnel

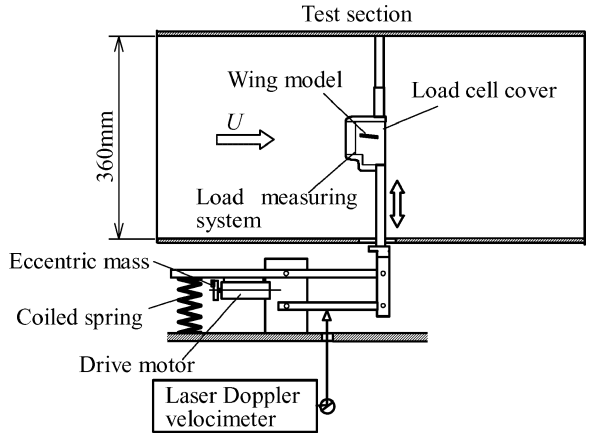

b) Driving mechanism for heaving

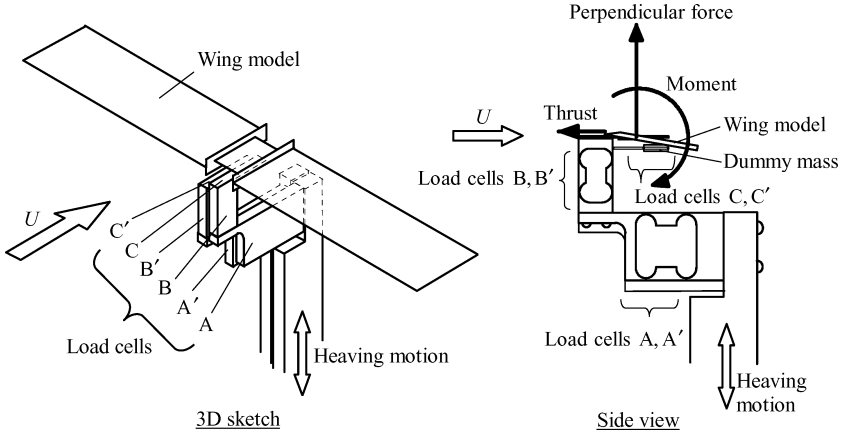

c) Load measuring device

Fig. 1 Driving mechanism for heaving in the wind tunnel and load measuring device.

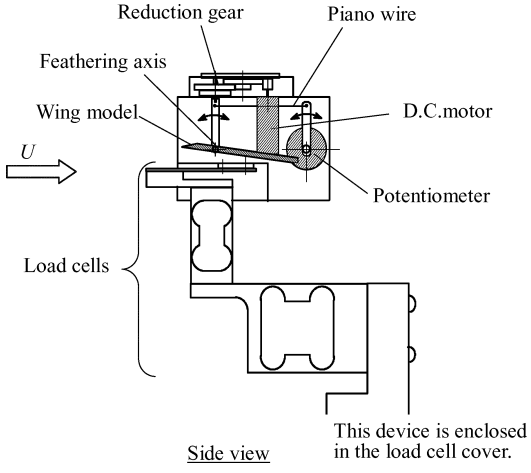

Fig. 2 Driving mechanism for feathering.

and the second harmonic oscillation is introduced only in the feathering motion.

The heaving amplitude h_1 can be determined by integrating the vertical acceleration measured by the dummy load cell, and the feathering amplitudes θ_1 and θ_2 are obtained by analyzing the time series of still pictures obtained with a stroboscopic camera.

By normalizing with the product of dynamic pressure $\frac{1}{2}\rho U^2$ and S for forces and Sc for moment, all forces and moment are expressed in nondimensional aerodynamic coefficients C_P, C_T, C_L, C_D, and C_M.

Results and Discussion

Steady-State Aerodynamic Characteristics

Shown in Table 1 and Figs. 6a and 6b are steady-state aerodynamic characteristics of airfoil models 1–8 presented in Fig. 4. The maximum lift coefficient $C_{L\max}$ is the largest for the airfoil 6, and it is the smallest for the airfoil 1. The minimum drag coefficient $C_{D\min}$ is the largest for the airfoil 6. As can be seen in Table 1 and the polar curves (Fig. 6b), the maximum lift-to-drag ratio is comparatively

large for the airfoils 4 and 5, and it is the smallest for the airfoil 1. Either by making the leading edge sharp, airfoil 2, or by attaching a flat chin, airfoil 3, the lift-to-drag ratio is improved as much as those of airfoils 4 and 5. For the dragonfly, the inboard wing (airfoil 7), which is highly cambered, is mainly responsible to support the weight of the body and is, thus, superior to the outboard wing (airfoil 8) with respect to the maximum lift coefficient. On the other hand, the outboard wing (airfoil 8), which is slightly cambered, is liable to generate a thrust, and therefore, it is formed to be lower minimum drag coefficient than that of the inboard wing (airfoil 7). The maximum lift-to-drag ratio $(L/D)_{\max}$ of airfoil 7 is similar to that of circular cambered airfoils, airfoils 4 and 5, and the $(L/D)_{\max}$ of airfoil 8 is larger than that of flat plate (airfoil 1). This preferable characteristic of the corrugated airfoil in low-Reynolds-number flow appears more remarkably in the wing with a sharp leading edge, and the characteristics of the other airfoils are consistent with the results obtained in the thinner wings as given in Refs. 1 and 2.

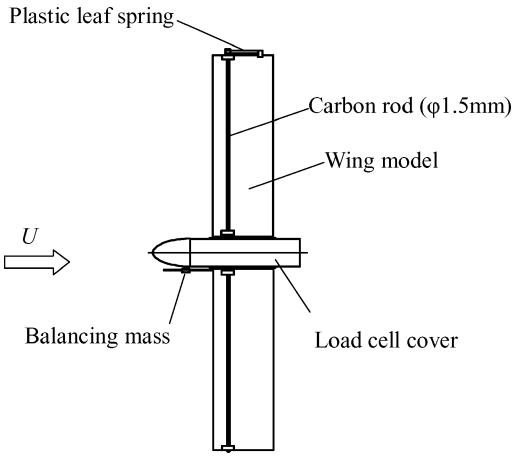

Fig. 3 Driving mechanism for a combined motion of heaving and feathering.

Unsteady Aerodynamic Characteristics

As stated before, the unsteady aerodynamic characteristics of eight wings in heaving and/or feathering oscillation are obtained.

Table 1 Aerodynamic characteristics of stationary airfoils

					α, deg[e]	
Airfoil no.	a_0[a]	$C_{L\max}$[b]	$C_{D\min}$[c]	$(L/D)_{\max}$[d]	$C_{L\max}$	$(L/D)_{\max}$
1	6.6	0.70	0.058	3.9	30	6
2	5.2	0.85	0.057	5.9	16	6
3	6.1	0.93	0.058	5.3	20	12
4	6.6	0.91	0.076	5.6	12	6
5	7.0	1.18	0.101	5.6	12	8
6	8.4	1.44	0.129	4.5	16	14
7	5.9	0.95	0.097	5.1	14	10
8	6.4	0.73	0.068	4.2	14	8

[a] a_0 = two-dimensional lift slope (α = 2–4 deg).
[b] $C_{L\max}$ = maximum lift coefficient.
[c] $C_{D\min}$ = minimum drag coefficient.
[d] $(L/D)_{\max}$ = maximum lift-to-drag ratio.
[e] α = angle of attack.

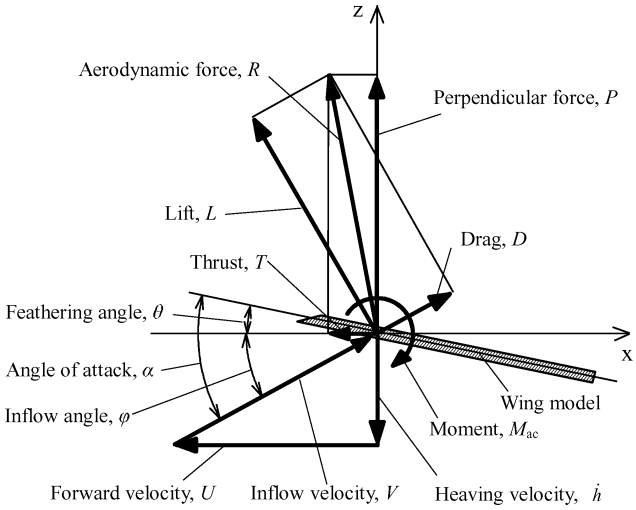

Fig. 5 Aerodynamic components of a wing model.

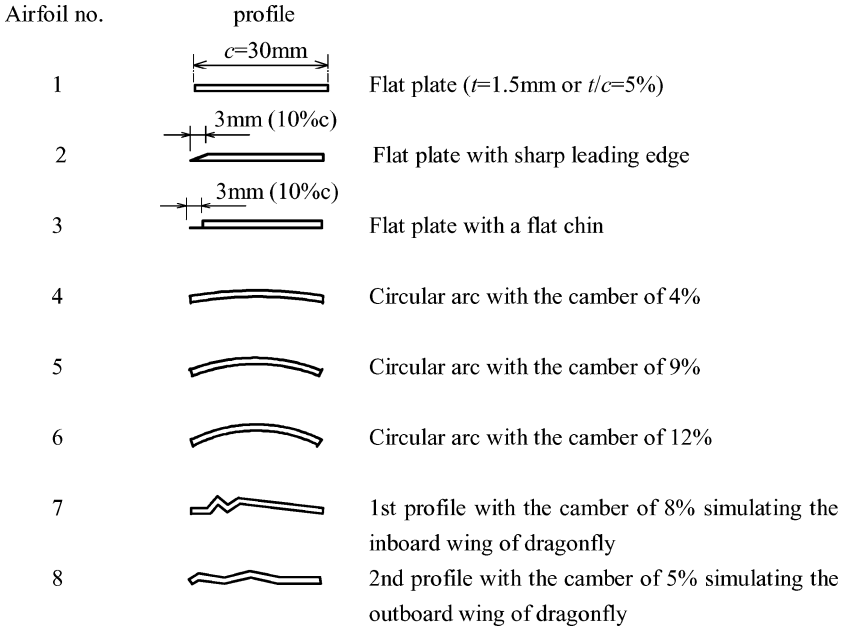

Fig. 4 Tested airfoils.

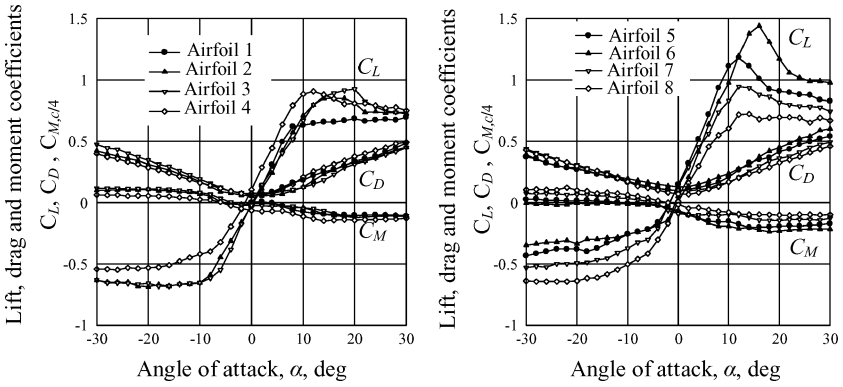

a) Aerodynamic characteristics vs angle of attack α

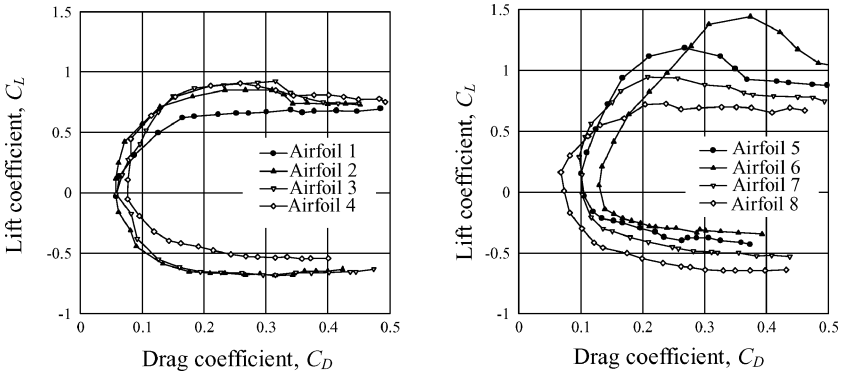

b) Polar curves

Fig. 6 Steady-state aerodynamic characteristics of airfoils ($Re = 7.6 \times 10^3$).

The frequency contained in measured aerodynamic forces and moment was almost twice the frequency of heaving and feathering oscillation. Because much higher frequency could not be distinguished from mechanical oscillation, a low-pass filter that has the corner frequency of 30 Hz was installed in the data processing.

Heaving Motion of a Flat Plate

Shown in Fig. 7 are time histories of heaving amplitude, angle of attack, aerodynamic coefficients of perpendicular force C_P, propulsive force, or thrust C_T and moment C_M about $c/4$ point for the flat plate (airfoil 1). The pitch angle of the model was fixed at $\theta = 6$ deg, the flow speed was also fixed at the Reynolds number of $Re = 7.60 \times 10^3$, and the model was sinusoidally oscillated in vertical direction with the amplitude-to-chord length ratio of $h_1/c = 0.47$ and the reduced frequency at $k = c\omega/2U = 0.31$.

The preceding aerodynamic force and moment coefficients can be shown as a function of angle of attack $\alpha = \theta + \varphi = \theta + \dot{h}/U$. Shown in Figs. 8a–8e are aerodynamic force and moment coefficients of the flat plate (airfoil 1) in heaving motion. Because of the large variation in angle of attack a, mainly in the range of $\alpha > 0$, the perpendicular force C_P is positive in the wide range of α. The thrust is mostly negative, which shows that the forward component of the lift does not exceeds the backward component of the drag caused by the large friction drag at low Reynolds number and the stall at high angles of attack caused by the heaving motion. The moment is represented by much higher harmonics and is mostly negative. As seen in Fig. 8a, because the C_P-α curve traces clockwise rotation, the work of heaving motion requires a positive power. The C_T-α curve and C_M-α curve in Figs. 8b and 8c almost trace anticlockwise rotation. The loci of data points in Fig. 8b resemble a Fig. 8 at the small pitch angle θ_0. The thrust and moment in the heaving motion do not require any power because the motion is only in the perpendicular direction to the thrust.

Shown in Figs. 8d and 8e are lift and drag coefficients vs angle of attack $C_L(\alpha)$ and $C_D(\alpha)$ for the flat plate (airfoil 1) in heaving

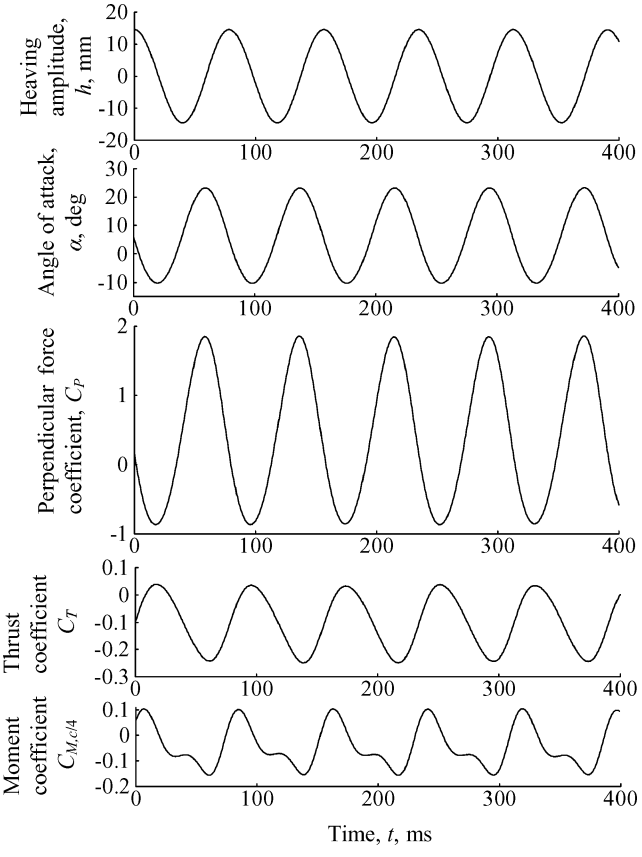

Fig. 7 Time histories of heaving and aerodynamic force and moment coefficients of the flat plate (airfoil 1) ($Re = 7.6 \times 10^3$, $\theta_0 = 6$ deg, $h_1/c = 0.47$, and $k = 0.31$).

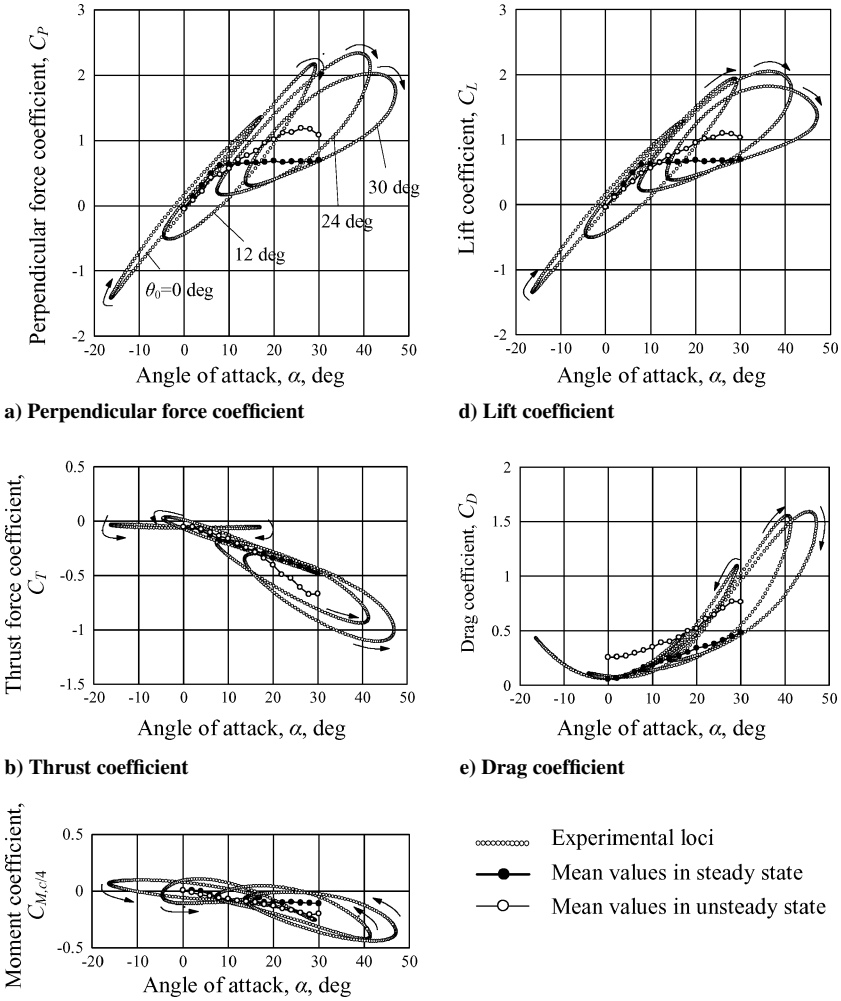

Fig. 8 Aerodynamic force and moment coefficients of the flat plate (airfoil 1) in heaving motion ($Re = 7.6 \times 10^3$, $h_1/c = 0.47$, and $k = 0.31$).

motion at various pitch angles. It is interesting to find that 1) as the pitch angle θ_0 increases the maximum lift coefficient $C_{L\max}$ increases to the peak value, which is almost three times the steady-state value at $\theta_0 = 24$ deg and then the $C_{L\max}$ decreases, and 2) clockwise hysteresis is observed in every case.

In Figs 8a–8e, large open circle symbols represent mean aerodynamic forces and moment $C_{P,0}$, $C_{T,0}$, and $C_{M,0}$. It can be seen that mean forces and moment in heaving motion deviate from their steady-state values, designated by large solid circles, at higher angles of attack beyond the steady-state stall angle. And mean drag coefficient $C_{D,0}$ is larger than steady-state value at all angles of attack tested.

Shown in Figs. 9a–9c are a series of perpendicular force coefficient C_P as a function of the mean pitch angle θ_0 for the flat plate (airfoil 1) in heaving motion with a combination of two inflow angles $\varphi = \tan^{-1}(\dot{h}/V) = 9$ and 16 deg and various values of reduced frequency k. Changing the reduced frequency k and the amplitude ratio of heaving oscillation h_1/c, or inflow angle φ defined by Eq. (4), every component of Fourier expansion series of aerodynamic forces and moment will be given as follows:

$$C_P = C_{P,0} + C_{P,1}\cos(\omega t + \psi_{P,1}) + C_{P,2}\cos(2\omega t + \psi_{P,2})$$

$$C_T = C_{T,0} + C_{T,1}\cos(\omega t + \psi_{T,1}) + C_{T,2}\cos(2\omega t + \psi_{T,2})$$

$$C_M = C_{M,0} + C_{M,1}\cos(\omega t + \psi_{M,1}) + C_{M,2}\cos(2\omega t + \psi_{M,2}) \quad (6)$$

where the constants with subscript 0 or zeroth-order values are considered to be mean values and the phase shifts $\psi_{P,1}$, $\psi_{P,2}$, $\psi_{T,1}$, $\psi_{T,2}$, $\psi_{M,1}$, and $\psi_{M,2}$ are phase differences from that of the heaving height h. The mean perpendicular force coefficient $C_{P,0}$ increases with the increase in mean pitch angle θ_0 except at larger pitch angles $\theta_0 > 20$ deg. Its rate of increase reduces beyond $\theta_0 = 20$ deg, and its value decreases with lowering of the reduced frequency k or the inflow angle φ. On the other hand, the amplitude of the first harmonic $C_{P,1}$ decreases with the increase in mean pitch angle θ_0, and it is remarkable when $k = 0.12$. A large increment in $C_{P,1}$ is observed when the inflow angle φ was changed from $\varphi = 9$ to 16 deg and its rate is in proportion to the φ. The phase shift from that of heaving in the first harmonic $\psi_{P,1}$ also increases with the increase in mean pitch angle θ_0 except when $k = 0.12$ and $\varphi = 9$ deg. The amplitude of second harmonic $C_{P,2}$ is very small in comparison with $C_{P,1}$. Other quantities C_T and C_M show similar trends with those of the C_P.

Feathering Motion of a Flat Plate

The feathering motion of the flat plate (airfoil 1) was conducted at nearly the same Reynolds number ($Re = 8.0 \times 10^3$) and reduced frequency ($k = 0.31$) to keep the same amplitude with that of the heaving angle $\theta \cong (\dot{h}/V)$. Shown in Figs. 10a and 10b are lift coefficient C_L and drag coefficient C_D, respectively. The results are almost the same as those shown in Figs. 8d and 8e, respectively. The angle of attack and lift coefficient are also expressed by Fourier coefficients as follows:

$$\alpha = \alpha_0 + \alpha_1\cos(\omega t), \qquad C_L = C_{L,0} + C_{L,1}\cos(\omega t + \psi_{L,1}) \quad (7)$$

where the angle of attack should be considered $\alpha = \tan^{-1}(\dot{h}/U)$ for heaving motion and $\alpha = \theta$ for feathering motion. Shown in

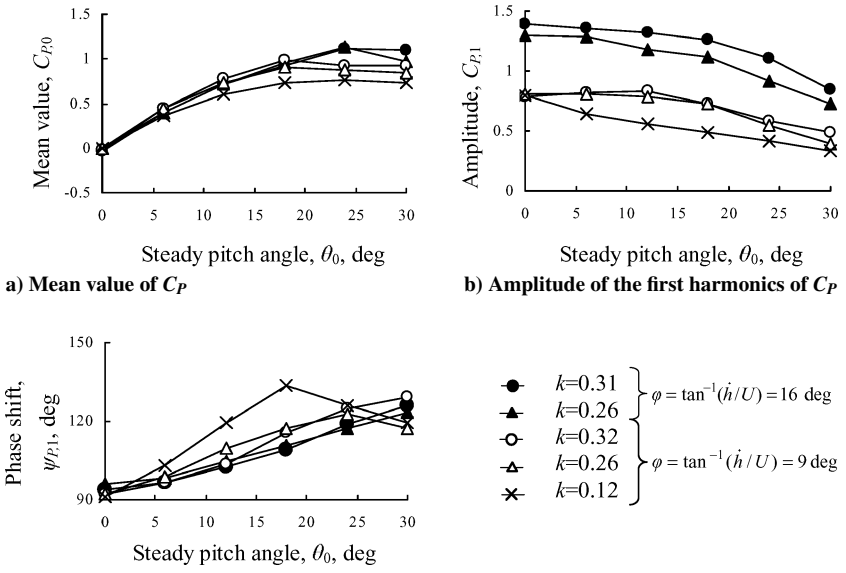

a) Mean value of C_P **b) Amplitude of the first harmonics of C_P**

c) Phase shift of the first harmonics of C_P

Fig. 9 Perpendicular force of the flat plate (airfoil 1) with respect to reduced frequency and heaving amplitude.

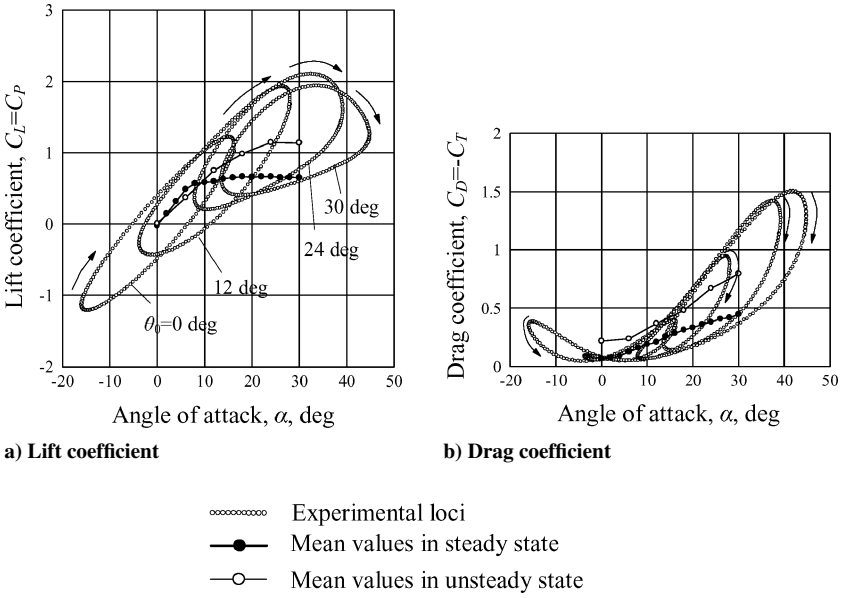

a) Lift coefficient **b) Drag coefficient**

Fig. 10 Aerodynamic force coefficients of the flat plate (airfoil 1) in feathering motion ($Re = 8.0 \times 10^3$, and $k = 0.31$).

Figs. 11a–11c are mean values, amplitudes, and phase shifts of the preceding first harmonics of lift coefficient for heaving and feathering motions.

A noticeable difference between the heaving and feathering motions is shown in the phase shift. By conducting model tests with feathering wings, Gangwani[15] made it clear that flow separation caused a large phase advance. However, as Fig. 11c shows in heaving oscillation, the phase shift was small in comparison with that of feathering oscillation.

Given in Table 2 are the maximum or minimum values of the aerodynamic coefficients of wings in heaving and feathering oscillations. As this table shows, appreciable differences are recognized in the maximum and minimum values of aerodynamic coefficients between the heaving and feathering motions of the flat plate (airfoil 1). The maximum thrust coefficient $C_{T\,\max}$ is positive in heaving motion, but it is negative in feathering motion because the lift, which is normal to the relative flow velocity, does not tilt forward during the feathering motion about the ac axis.

Table 2 Aerodynamic characteristics of unsteady airfoil

Motion	Airfoil no.	$C_{P\,\max}$[a]	$C_{T\,\max}$[b]	$C_{L\,\max}$[c]	$C_{D\,\min}$[d]	$C_{M\,\min}$[e]
Heaving	1	2.31	0.031	2.03	0.053	−0.44
	2	2.46	0.069	2.03	0.019	−0.42
	3	2.48	0.064	2.16	0.023	−0.41
	4	2.56	0.065	2.25	0.035	−0.49
	5	2.68	0.084	2.34	0.038	−0.56
	6	2.80	0.050	2.47	0.080	−0.52
	7	2.58	0.071	2.28	0.046	−0.47
	8	2.37	0.041	2.10	0.037	−0.45
Feathering	1	2.09	−0.038	2.09	0.038	−0.61
Combined heaving and feathering	2	2.33	0.14	2.09	0.033	——

[a] $C_{P\,\max}$ = maximum perpendicular force coefficient.
[b] $C_{T\,\max}$ = maximum thrust coefficient.
[c] $C_{L\,\max}$ = maximum lift coefficient.
[d] $C_{D\,\min}$ = minimum drag coefficient.
[e] $C_{M\,\min}$ = minimum moment coefficient.

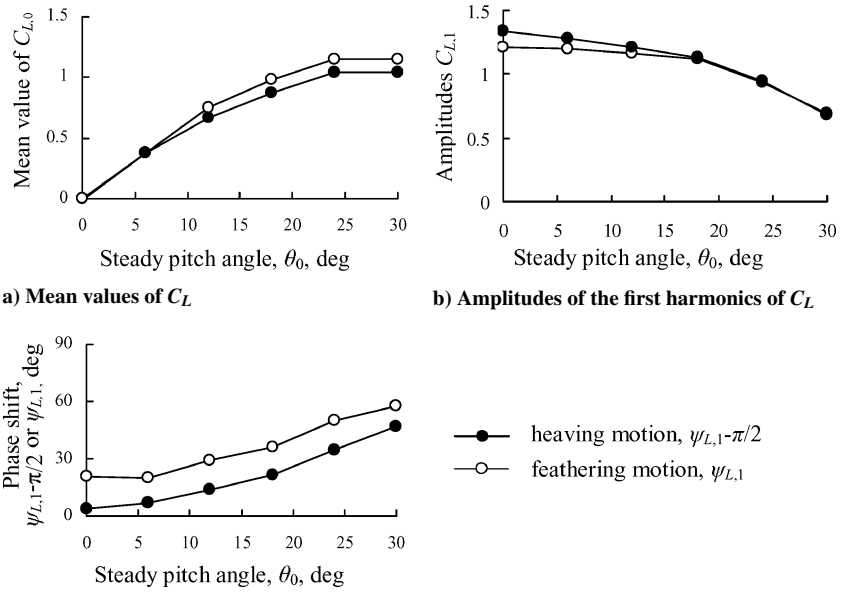

a) Mean values of C_L

b) Amplitudes of the first harmonics of C_L

c) Phase shifts of the harmonics of C_L

Fig. 11 Quantities related to the first harmonics of lift coefficient.

Effects of Profile Configuration

Shown in Figs. 12a–12c are aerodynamic force and moment coefficients of the wing with circular arc airfoil with 9% camber (airfoil 5) in heaving motion. The maximum perpendicular force coefficient $C_{P\max}$ (Fig. 12a) is larger than that of the flat plate (Fig. 8a). The $C_{P\max}$ for circular arc airfoil in heaving motion shows a similar trend with the maximum lift coefficient $C_{L\max}$ in steady state, which is larger than that of the flat plate. The $C_{L\max}$ for the wing with circular arc airfoil with 9% camber in steady state is about 1.7 times as much as for the flat plate, but $C_{P\max}$ in heaving motion increases only by 16%. The thrust coefficient C_T is partially positive in $-12\,\text{deg} \le \theta_0 \le 12\,\text{deg}$ and $\dot{h}/U > 0$ (or downstroke), and it is slightly larger than that of the flat plate shown in Fig. 8b. The absolute value of the moment coefficient $C_{M,c/4}$ is larger than that of the flat plate as shown in Fig. 8c.

In Fig. 12, mean aerodynamic force coefficients $C_{P,0}$, $C_{T,0}$ and moment coefficient $C_{M,0}$, represented by large open circle symbols, deviate at higher angle of attack from their steady-state values, represented by large solid circle symbols. The nonlinearity of lift and moment curves seen in steady state becomes more linear in $C_{P,0}$ and $C_{M,0}$ curves in heaving motion. And the slope of $C_{P,0}$ in heaving motion is smaller than that of C_L in steady state.

Differences in unsteady aerodynamic characteristics caused by profile configuration changes are summarized and discussed here. Table 2 shows the maximum and minimum values of these characteristics, and the Fourier coefficients of perpendicular force C_P, thrust C_T, and moment C_M are shown in Figs. 13a–13c, respectively. The plain flat plate is inferior to wings with other airfoils as far as the maximum perpendicular force and lift coefficients are concerned. Airfoils 4–6 and 7, circular arc and dragonfly airfoils, respectively, provided large perpendicular force. The circular arc airfoil with 12% camber provided the largest value in the preceding coefficients. This conclusion is affirmative with steady-state aerodynamic characteristics shown in Table 1. The sharp leading edges, as with the airfoils 2 and 3, are effective to increase the thrust. Airfoils 5 and 7, cambered and dragonfly airfoils respectively, produced greater thrust coefficients than other airfoils.

As seen in Fig. 13a, the general trends of the mean values of perpendicular force coefficient C_P are not different from those of the steady state. The circular arc airfoil with 12% camber (airfoil 6) had the maximum mean value of $C_{P,0}$ same as in the steady state. On the contrary, the amplitudes of the first harmonic $C_{P,1}$ for the circular arc airfoil with 12% camber are lower than those of the other airfoils. The flat plate has the maximum $C_{P,1}$ only when $\theta_0 = 0$. The

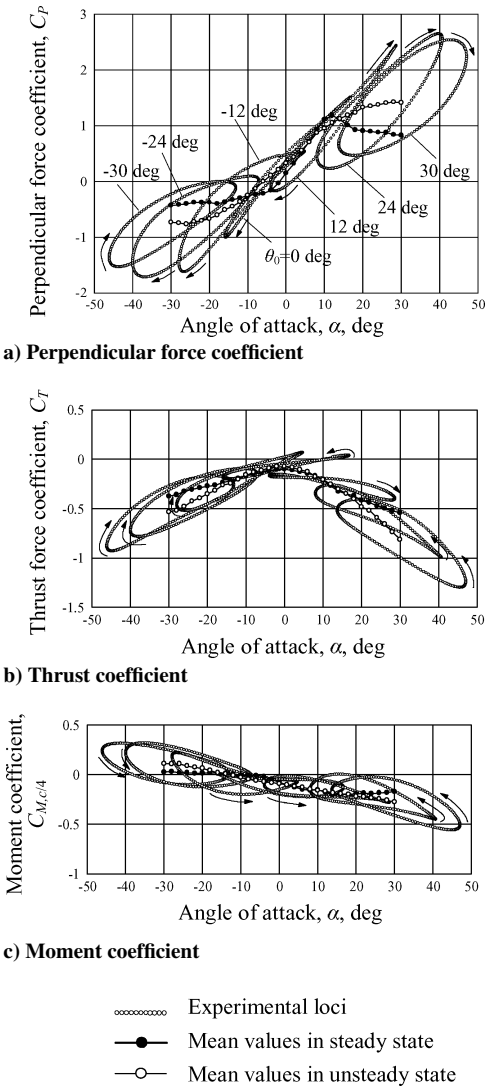

a) Perpendicular force coefficient

b) Thrust coefficient

c) Moment coefficient

Fig. 12 Aerodynamic force and moment coefficients of the wing with circular arc airfoil with 9% camber (airfoil 5) ($Re = 7.8 \times 10^3$, $h_1/c = 0.47$, and $k = 0.32$).

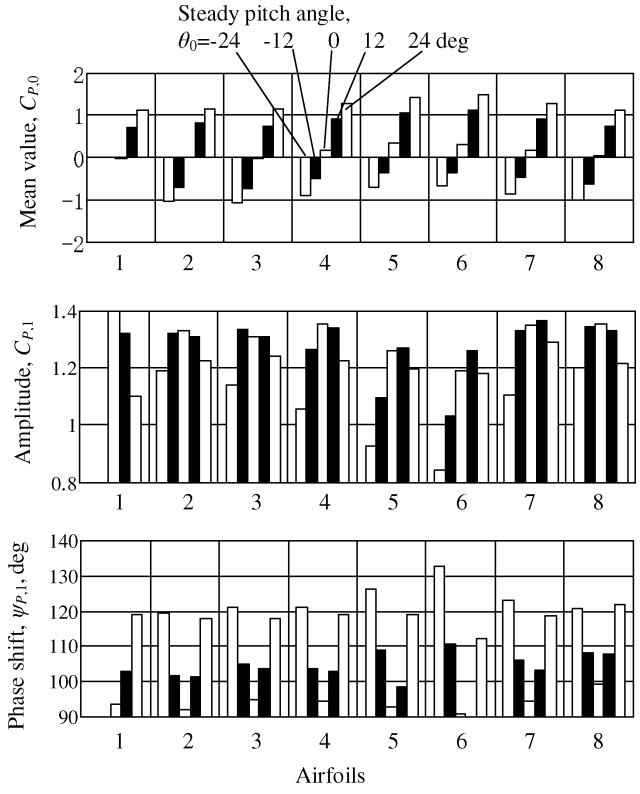

a) Perpendicular force coefficient

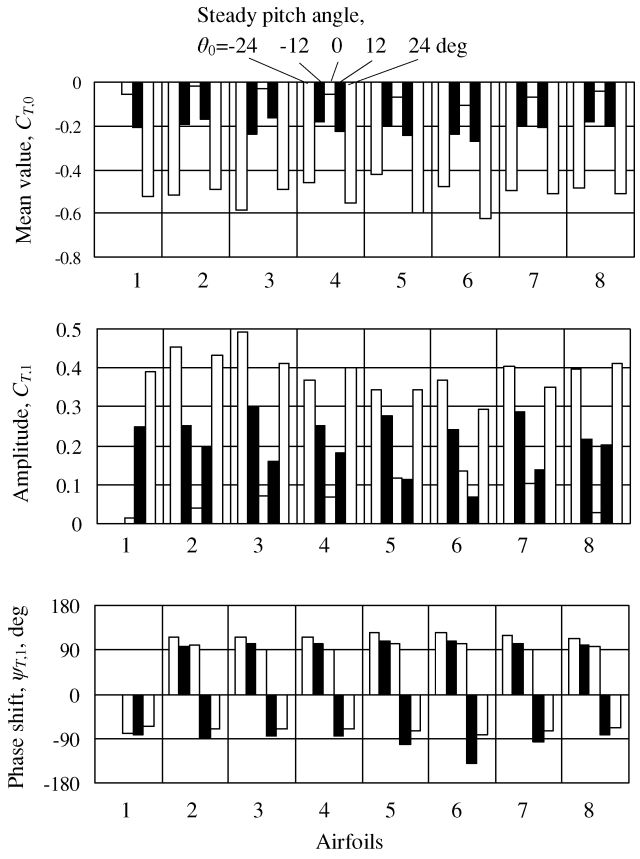

b) Thrust coefficient

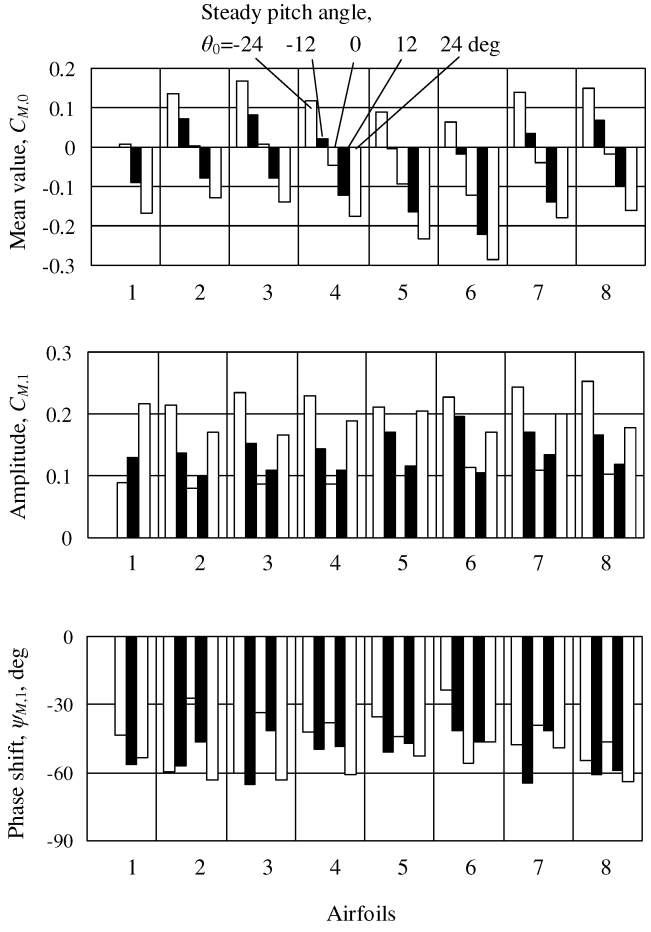

c) Moment coefficient

Fig. 13 Variation of Fourier coefficient for force and moment coefficients of eight airfoils.

airfoils with sharp leading edge, airfoils 2 and 3, show high $C_{P,1}$ except when $\theta_0 = 0$. Furthermore, the dragonfly airfoils, airfoils 7 and 8, show high $C_{P,1}$ for large $|\theta_0|$ or $\theta_0 > 12$ deg and $\theta_0 < -12$ deg, respectively. The phase shift with respect to the heaving motion $\psi_{P,1}$ starts from 90 deg at the zero pitch angle ($\theta_0 = 0$) and increases with the increase in the absolute value of pitch angle $|\theta_0|$. In the negative pitch angle $\theta_0 < 0$ of the circular arc airfoils, the phase shift $\psi_{P,1}$ increases with the camber, whereas in the positive pitch angle $\theta_0 > 0$ this tendency goes backward.

The amplitudes of the second harmonics in the Fourier coefficients were not picked up because these values did not display distinctive characteristics among the profile configurations tested.

As can be seen from Fig. 13b, thrust coefficient, the mean value $C_{T,0}$ is negative for every θ_0 and increases negatively with $|\theta_0|$ along with the increase in drag coefficient. The amplitude of the first harmonics of thrust coefficient $C_{T,1}$ exceeds the absolute value of $C_{T,0}$ for some range of pitch angle θ_0. As a matter of fact, the thrust is approximately given by the forward tilt component of the lift $[t \cong l\dot{h}/V - d \cong a(\dot{h}/V)^2 - d]$, and thus the thrust should be expressed by the second harmonics in the Fourier expansion series. Almost all airfoils produce positive thrust within the pitch angle range of -12 deg $\leq \theta_0 < 12$ deg (except the airfoil 1 at $\theta_0 = 0$) and the thrust is larger at $\theta_0 = -12$ deg than at $\theta_0 = 12$ deg. However, the thrust is discarded in stalled range, and the second harmonics $C_{T,2}$ is small in comparison with $C_{T,1}$ in low-Reynolds-number flow because the drag is given by the second harmonics of angle of attack $d \propto (\dot{h}/V)^2$. The phase shift of the thrust coefficient $\psi_{T,1}$ increases with the increment of the absolute value of pitch angle $|\theta_0|$, like the phase shift of perpendicular force coefficient $\psi_{P,1}$. In the positive pitch angle $\theta_0 > 0$, the phase shift $\psi_{T,1}$ exceeds 180 deg, and the negative value of the phase shift $\psi_{T,1}$ decreases with the increment of airfoil camber.

As can be seen from Fig. 13c, the mean value of the moment coefficient $C_{M,0}$ shows the similar trend to that of steady state. The differences of the first harmonics $C_{M,1}$ in various airfoils are small because the influence of the added mass is large. The phase shift of the moment coefficient $\psi_{M,1}$ is negative and increases with the increment of the camber of the circular arc airfoils, airfoils 4–6, except for the pitch angle when $\theta_0 = 0$.

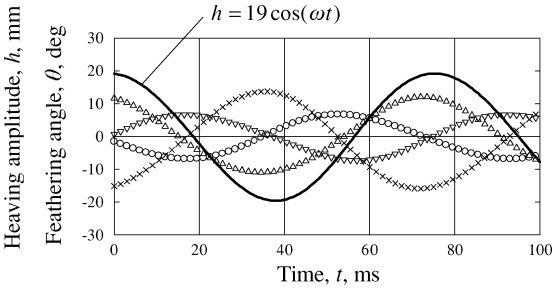

a) Heaving and feathering motions

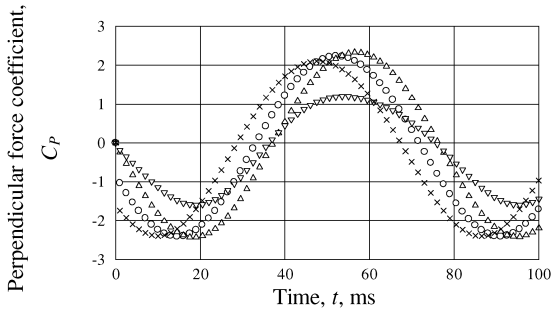

b) Perpendicular force coefficient

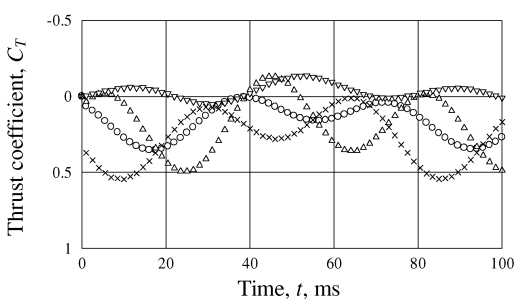

c) Thrust coefficient

Fig. 14 Time variation of the aerodynamic force coefficients of the flat plate with sharp leading edge (airfoil 2) in a combined motion of heaving and feathering ($Re = 8.0 \times 10^3$, $h_1/c = 0.68$, and $k = 0.32$): ○, $\psi_\theta = 90$ deg, $\theta_1 = 6.8$ deg; ▽, $\psi_\theta = -93$ deg, $\theta_1 = 6.7$ deg; △, $\psi_\theta = 8$ deg, $\theta_1 = 11.5$ deg; and ×, $\psi_\theta = -172$ deg, $\theta_1 = 14.8$ deg.

Combination of Heaving and Feathering Motions

A flat plate with sharp leading edge (airfoil 2) was oscillated sinusoidally in a combined motion of heaving and feathering. The heaving motion was actively driven, but, as stated before, the feathering motion was passively provided as a free feathering motion tuned with the resonant frequency by changing both the position of the center of gravity with respect to the feathering axis and the stiffness of the leaf spring installed on the feathering axis.

Figures 14a–14c show experimental data of the wing with airfoil 2 when it was in the combined motion of heaving and feathering: heaving amplitude and resulted feathering angle, perpendicular force coefficient C_P, and thrust coefficient C_T for various phase differences ψ_θ. The following observation are made:

1) For a given heaving amplitude of $h_1/c = 0.68$ and the reduced frequency of $k = 0.32$, the largest amplitude of perpendicular force and thrust are obtained at the phase shift of $\psi_\theta = 8$ deg with the feathering angle of $\theta_1 = 11.5$ deg.

2) The smallest amplitude of perpendicular force and thrust are produced by the phase difference of $\psi_\theta = -93$ deg with the feathering angle of $\theta_1 = 6.7$ deg.

3) The positive mean thrust is obtained only with the preceding second condition. This positive thrust is obtained mainly from the forward component of the normal force acting on the plate, which is tilted forward in both downward and upward heaving. This result coincides with the flapping phase of the insect in forward flight.[16,17]

Conclusions

From the wind-tunnel tests of wings with various airfoils in unsteady motion at low Reynolds number, the following results can be obtained:

1) By applying the heaving motion, the maximum lift or perpendicular force coefficients increase remarkably. These forces are, as a matter of course, strongly related to the flow separation with some phase advance to the angle of attack.

2) By either sharpening the leading edge or increasing the airfoil camber, the maximum lift or perpendicular force coefficients increase appreciably. The corrugation of the airfoil is also effective in improving the aerodynamic characteristics of the flat plate. Generally, the effect of the variations of airfoil configuration on their mean values is little difference between steady and unsteady motions. However, the effect of the sharp leading edge and the corrugated airfoil on the amplitude of the first harmonic Fourier coefficient is appreciably larger than that of the airfoil camber.

3) Because the angle of attack α can be given by θ in feathering motion and by $\dot{h}/U$ in heaving motion, the derived unsteady aerodynamic forces and moment have different phase lags between the preceding feathering and heaving motions, although their magnitudes are nearly equal.

4) The maximum thrust is partially positive in heaving motion, but it is negative in feathering motion. The optimal combination of heaving and feathering motions for the positive mean thrust can be obtained by having the phase difference of $\psi_\theta = -90$ deg.

The next step of experimental tests is to investigate the effects of change of planform on the steady and unsteady aerodynamic characteristics of thin wings moving in low-Reynolds-number flow.

Acknowledgment

The authors are grateful to Shojiro Shindo for the support to write this paper.

References

[1]Okamoto, M., Yasuda, K., and Azuma, A., "Aerodynamic Characteristics of the Wings and Body of a Dragonfly," *Journal of Experimental Biology*, Vol. 199, 1996, pp. 281–294.

[2]Azuma, A., Okamoto, M., and Yasuda, K., "Aerodynamic Characteristics of Wing at Low Reynolds Number," *Conference on Fixed, Flapping and Rotary Wing Vehicles at Very Low Reynolds Numbers*, edited by T. J. Mueller, Vol. 195, Progress in Astronautics and Aeronautics, AIAA, Reston, VA, 2001, pp. 341–398.

[3]Sunada, S., Yasuda, T., Yasuda, K., and Kawachi, K., "Comparison of Wing Characteristics at an Ultralow Reynolds Number," *Journal of Aircraft*, Vol. 39, No. 2, 2002, pp. 331–338.

[4]Dickinson, M. H., and Götz, K. G., "Unsteady Aerodynamic Performance of Model Wings at Low Reynolds Numbers," *Journal of Experimental Biology*, Vol. 174, 1993, pp. 45–64.

[5]Dickinson, M. H., "The Effects of Wings Rotation on Unsteady Aerodynamic Performance at Low Reynolds Numbers," *Journal of Experimental Biology*, Vol. 192, 1994, pp. 179–206.

[6]Sunada, S., Kawachi, K., Matsumoto, M., and Sakaguchi, A., "Unsteady Force on a Two-Dimensional Wing in Plunging and Pitching Motions," *AIAA Journal*, Vol. 39, No. 7, 2001, pp. 1230–1239.

[7]Zanker, J. M., and Götz, K. C., "The Wing Beat of Drosophila *Melanogaster*.II. Dynamics," *Philosophical Transactions of the Royal Society of London, Series B*, Vol. 327, 1990, pp. 19–44.

[8]Ellington, C. P., van Den Berg, W. A. P., and Thomas, A. L. R., "Leading-Edge Vortices in Insect Flight," *Nature*, Vol. 384, Dec. 1996, pp. 626–630.

[9]Lehmann, F. O., and Dickinson, M. H., "The Control of Wing Kinematics and Flight Forces in Fruit Flies (*Drosophila Sp.*)," *Journal of Experimental Biology*, Vol. 201, 1998, pp. 385–401.

[10]Dickinson, M. H., Lehmann, F. O., and Sane, S. P., "Wing Rotation and the Aerodynamic Basis of Insect Flight," *Science*, Vol. 284, No. 18, 1999, pp. 1954–1960.

[11]Sane, S. P., and Dickinson, M. H., "The Aerodynamic Effects of Wing Rotation and a Revised Quasi-Steady Model of Flapping Flight," *Journal of Experimental Biology*, Vol. 205, 2002, pp. 1087–1096.

[12]Usherwood, J. R., and Ellington, C. P., "The Aerodynamics of Revolving Wings. I. Model Hawkmoth Wings," *Journal of Experimental Biology*, Vol. 205, 2002, pp. 1547–1564.

[13]Usherwood, J. R., and Ellington, C. P., "The Aerodynamics of Revolving Wings. II. Propeller Force Coefficient from Mayfly to Quail," *Journal of Experimental Biology*, Vol. 205, 2002, pp. 1565–1576.

[14]Srygley, R. B., and Thomas, A. L. R., "Unconventional Lift-Generating Mechanisms in Free-Flying Butterflies," *Nature*, Vol. 420, No. 12, 2002, pp. 660–664.

[15]Gangwani, S. T., "Synthesized Airfoil Data Method for Prediction of Dynamic Stall and Unsteady Airloads," *Vertica*, Vol. 8, No. 2, 1984, pp. 93–118.

[16]Azuma, A., and Watanabe, T., "Flight Performance of a Dragonfly," *Journal of Experimental Biology*, Vol. 137, 1988, pp. 221–252.

[17]Sato, M., and Azuma, A., "The Flight Performance of a Damselfly, *Ceriagron melanurun* Selys," *Journal of Experimental Biology*, Vol. 200, 1997, pp. 1765–1779.

A. Plotkin
Associate Editor